Electrochemical Study Of Passivated Oxide Film Formation On Carbon Steel And Its Interatcion With H_2O_2

W. Xu, J.C. Wren*
The University of Western Ontario, London, Ontario, Canada

Abstract

Carbon steel corrosion is an electrochemical process associated with the dissolution of Fe ions caused by breakdown of passivated films on the metal surface. It is one of the operational and safety challenges in nuclear industry. Water radiolysis produces highly reactive species in the presence of ionizing radiation, the environment in the reactor coolant system of CANDU nuclear plant. Water radiolysis products, in particular, H_2O_2, enhance the corrosion rate of carbon steel pipes used in the CANDU heat transport system. The corrosion kinetics is complex and depends on the physical and chemical properties of the steel surface and solution pH and redox conditions. The interaction of H_2O_2 with iron oxide/hydroxide films on carbon steel was studied by electrochemical and surface analytical techniques. Iron oxide/hydroxide films were grown potentiostatically for different lengths of time at various potentials and characterized using Electrochemical Impedance Spectroscopy (EIS). The interaction of oxide films with H_2O_2 was studied mainly at room temperature (limited study at higher temperatures) by monitoring the open circuit potential (or corrosion potential, E_{CORR}) as a function of exposure time to H_2O_2, and by performing EIS after different reaction times. Ex-situ Raman spectroscopy was also performed to characterize some of the films.

1. Introduction

Many of the operational and safety issues of nuclear power plants stem from the effects of radiation on the oxidation or corrosion of construction materials. Of particular concern are the effects of chemically reactive species produced by radiolysis of coolant water. Exposed to ionizing radiation (e.g. α, β and γ–radiation), water decomposes to yield a range of chemically reactive species: •OH, e_{aq}^-, H•, HO_2•, H_2, H_2O_2, H^+ [1]. The interaction of water radiolysis products and surfaces can be synergistic and the net effect is difficult to predict. Since water radiolysis produces both highly oxidizing and reducing species, it can influence the redox conditions in nuclear reactor coolant water and, hence, the corrosion kinetics of materials in contact with the water. For a reactive material such as carbon steel, the redox condition is established by the interactions between reactive radiolysis products and the steel surface, and the corrosion products produced by these reactions. Some radiolysis products can also decompose on the surface via a process not involving corrosion of metal and dissolved corrosion products can catalytically react with the radiolysis products. These processes can, in turn, affect the concentrations of the radiolysis products. An attempt to represent this synergistic circuit is shown in Figure 1.

To understand the complex synergistic effects and to develop a mechanistic model (a mixed electrochemical potential model coupled with reaction kinetics) for steel corrosion in radiation environments, a detailed understanding of interactions of oxide/hydroxide films and water radiolysis products is necessary. In the current study, oxide/hydroxide films on carbon steel were grown and characterized, and the interaction of H_2O_2 with oxide-covered carbon steel surfaces was monitored, by electrochemical techniques, such as cyclic voltammetry (CV) and electrochemical impedance spectroscopy

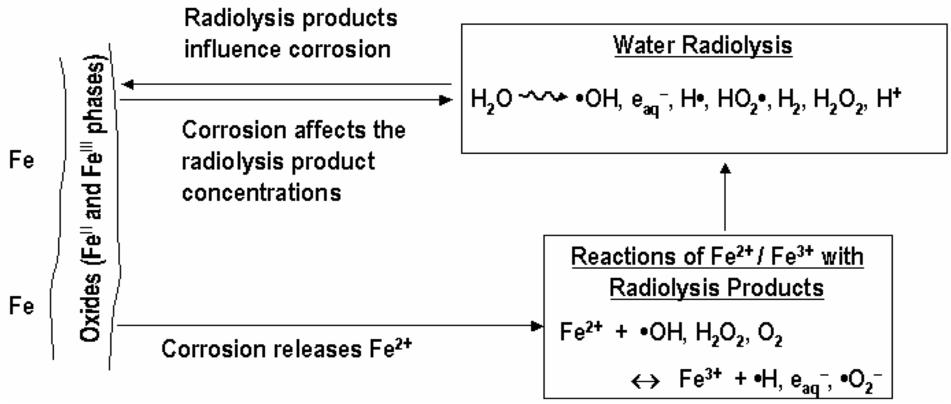

(EIS).

Figure 1: Schematic illustration of the synergistic interactions between water radiolysis and the corrosion of carbon steel.

2. Experimental

2.1. Electrochemical system

A standard three-electrode cell consisting of a working electrode, a reference electrode and a counter electrode, was used for all experiments. The working electrode was made by setting a 10-mm (in diameter) A516 Gr70 carbon steel disc in resin to control the surface area. Prior to each experiment, this electrode was polished manually with 600 and 800 grit silicon carbide papers, and polished residues were removed by sonicleaning in an acetone/methanol mixture for 5 minutes. The reference electrode was a saturated calomel electrode (SCE) and the counter electrode was a platinum mash. All potential measurements were made with or quoted against a SCE (242 mV verses NHE).

A Solarton model 1240 potentiostat and 1252-frequency response analyser were used in all electrochemical measurements. Corrware^{TM} and Corrview software (supplied by Scribner and Associates) were used for experiment control and data analysis. Electrochemical Impedance Spectroscopy (EIS) was performed by applying a 10 mV sinusoidal waveform potential at an open circuit potential over the frequency range 10^{-2} to 10^{4} Hz.

2.2. Solutions

Electrolyte used was 0.01 M borate buffer ($Na_2B_4O_7$) at pH 10.6 adjusted by NaOH (unless otherwise stated). Solutions were prepared with deionized water purified by a NANOpure Diamond UV ultra pure system from Barnstead International. In this manner, the water had a resistivity of 18.2 Nohm/cm. All solutions were AR purged for at least 20 minutes to minimize the effect of O_2 in solution.

The H_2O_2 solution used in these experiments was 30% by weight percentage. . The desired H_2O_2 concentration in the range of 10^{-4} to 10^{-2} M was obtained by adding a certain amount of this concentrated H_2O_2 to electrolyte.

2.3. Experimental Procedure

The experimental procedure used to study the electrochemical formation of oxide/hydroxide films on carbon steel and interactions of these films with H_2O_2 was present in Figure 2. All experiments were preceded by a cathodic cleaning on carbon steel working electrode at a potential of –1.1 V for 300 s, initially. Then, an iron oxide/hydroxide film was grown potentiostatically at a potential in the range –0.15 V to +0.4 V for 1 h, monitoring the currents and net charges (Step 1). Next, films were allowed to relax at open circuit potential (E_{CORR}) for about 20 minutes to a pseudo steady-state value (Step 2), Following with EIS (Step 3) to characterize the films formed. H_2O_2 solution was added so that the concentration of H_2O_2 in electrolytes was 10^{-3} M. the oxidation reaction on carbon steel surface is then monitored by measuring E_{CORR} and EIS, alternatively (Step 4 and 5).

Cyclic voltammetry was used to characterize all possible reactions on carbon steel surface and their corresponding reaction potentials in investigated range. It was obtained from the cathodic cleaning potential to various anodic limits at a scan rate at 5 $mV{\cdot}s^{-1}$, and was also conducted as a function of pH, temperature, electrode rotation speed and the numbers of scan cycles.

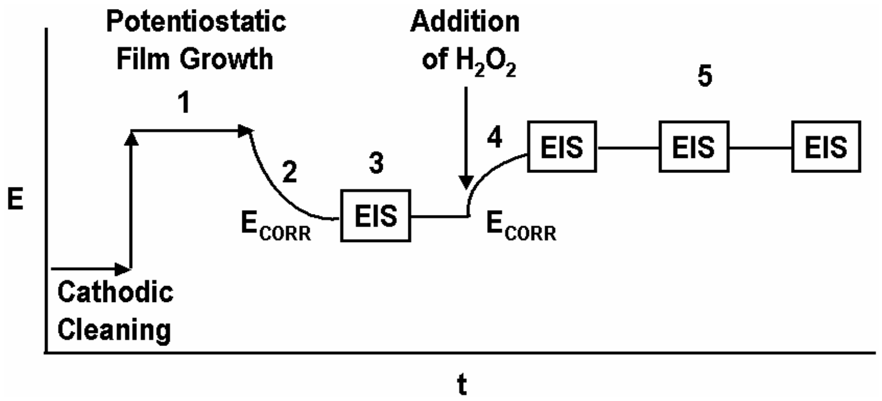

Figure 2: Schematic of the experimental Procedure used in this study.

3. Results and discussion

3.1. Cyclic Voltammetry

Tons of cyclic voltammetry experiments under different situations had been done in the past.

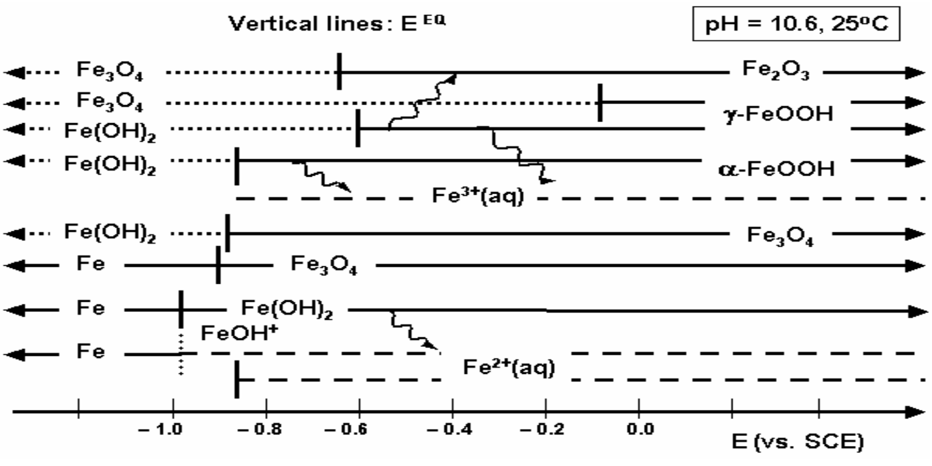

Figure 3: Schematics of equilibrium potentials (vs. SCE) for possible redox reactions on carbon steel. The short vertical lines indicate the equilibrium potentials for given

redox pairs at pH =10.6 and 25^{o}C. The curvy lines indicate potential non-electrochemical processes such as dissolution and phase transformations.

The purpose for these scans was to provide a basis for film growth potentiostatically and EIS experiments. Figure 3 summarizes the possible inter-conversions among iron and its oxide/hydroxide based on the data from Misawa [7,8].

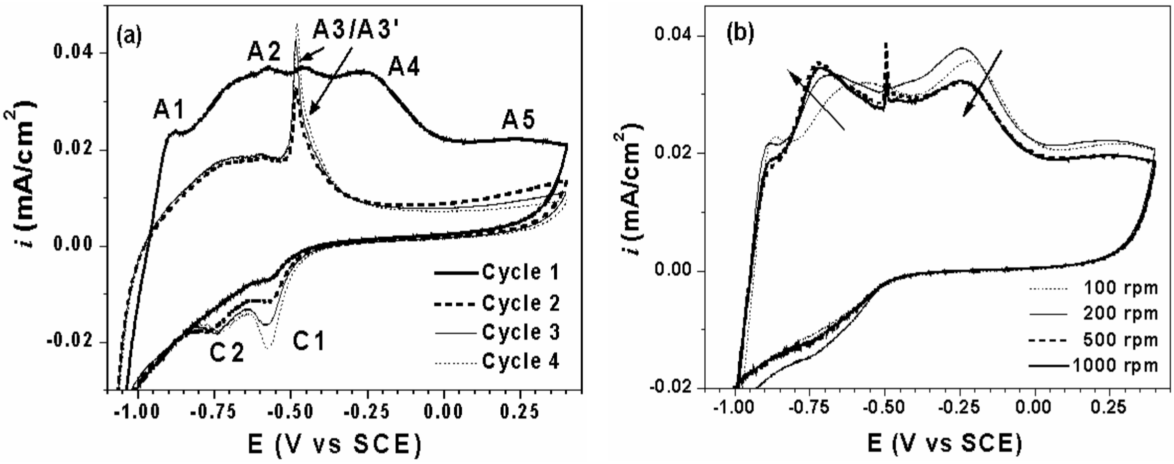

Figure 4: Cyclic Voltammetry recorded on carbon steel electrode in Ar-purged, 0.01 M sodium borate buffer solution at pH 10.6 and 25^{o}C at a scan rate of 5 mV/s: a) CVs obtained for different scan cycles (without rotation); and b) CVs of the first scan cycle obtained with various electrode rotation speeds. The arrows in b) indicate trends of the changes with an increase in rotation speed.

Figure 4(a) represents the influence of scan cycles without rotating the working electrode. In the first cycle, five indistinct peaks are observed, which is not a surprise considering the possible thermodynamic interactions. Similar behaviour is observed at other pH values [9,10, 11]. The charge input for cathodic and anodic scans could be obtained by integrating cathodic and anodic currents. The charge input for anodic scan is larger than that of cathodic scan indicates that the anodic products are either soluble or not completely reduced in cathodic scan. Subsequent cycles, performed without re-preparing the electrode surface, show a decrease in general reactivity, together with increases in a distinct anodic peak (A3/A3') and two cathodic peaks (C1 and C2).

The shoulder at ~ – 0.9 V (A1 in Figure 3a), which is only observed in the first cycle, can be attributed to the oxidation of H absorbed in the working electrode during the cathodic cleaning [11]. The broad anodic peak (A2) in the potential range – 0.9 V to – 0.6 V encompasses the active metal dissolution region within which formation of $Fe(OH)_2$, Fe_3O_4 and conversion of $Fe(OH)_2$ to α-FeOOH become thermodynamically possible. This peak is partially solved by varying scan rates. The commonly accepted mechanism for dissolution acknowledges the importance of intermediate oxidation states of Fe^{I} [12-18]:

$$Fe + OH^{-} \rightarrow [Fe(OH)_{ads} + e^{-}] \rightarrow FeOH^{+} + 2\,e^{-} \qquad (1)$$

$$FeOH^{+} + OH^{-} \rightarrow Fe\,(OH)_2 \qquad (2)$$

Thus, dissolution precedes $Fe(OH)_2$ formation on the surface. At pH 10.6, the potential for the anodic formation of $Fe(OH)_2$ from Fe is low (– 0 .973 V vs. SCE), thereby the equilibrium among the Fe^{II} species ($Fe^{2+} \leftrightarrows Fe(OH)^{+} \leftrightarrows Fe(OH)_2 \leftrightarrows Fe(OH)_3^{-}$) in the aqueous phase is fast. As $Fe(OH)_2$ could be transformed from Fe^{II} species that is adsorbed on carbon steel surface, $Fe(OH)_2$ formation could be rapid [19].

Figure 4(b) illustrates the influence of electrode rotation rate. It seems peak A2 (–0.9 V to –0.6 V) and peak A4 (–0.4 V to –0.1 V) are more or less related, and some soluble species may be involved. Evidences at lower [9,10] and higher [11] pH values suggests that active dissolutions are suppressed by formation of $Fe(OH)_2$ and/or Fe_3O_4. This could account for the increase in current observed on rotating electrodes over the potential range –0.9 V to –0.6 V The current in region A2 increases with electrode rotation rate indicating an increase in formation of Fe^{2+} species. As $Fe(OH)_2$ is soluble, dissolution occurs in competition with the formation of a $Fe(OH)_2$ film. An increase in rotation rate would increase $Fe(OH)_2$ dissolution. The overall amount of $Fe(OH)_2$ on carbon steel surface decreases as rotation rate increases. In contrast, the current for region A4 decreases with an increase in rotation rate implying that the anodic process is partially suppressed by a decrease in the availability of $Fe(OH)_2$. These observations, as well as the increase in current and the shift in peak position to more negative potentials observed with increasing pH (not shown), allow us to attribute peak A4 to the oxidation of Fe^{II} species to α-FeOOH. The equilibrium potential for the conversion of $Fe(OH)_2$ to α-FeOOH lies at a much more negative potential, indicating that the kinetics of this anodic process is slow. These claims are consistent with the claims of Guzman *et.al.* [20] and Hugot–LeGoff [8], who observed a current peak for this reaction at ~ –0.75 V in 1 M NaOH, and with the results of Ohtsuka et.al. [21], which suggested that the anodic oxidation of soluble Fe^{II} species resulted in the formation of a partially hydrated FeOOH (or $Fe(OH)_3$) layer.

In subsequent voltammetry cycles, Figure 4(a), the currents for region A2 and A4 are considerably reduced, which could be due to the formation of Fe_3O_4. Fe_3O_4 can form either directly from Fe metal or convert from Fe^{II} species, such as: $Fe(OH)_2$. Both of these reactions become thermodynamically feasible at the negative potential end in region A2. The fact That Fe_3O_4 is formed around this potential, and subsequently stays over the whole potential range scanned has been demonstrated by in-situ Raman Spectroscopy [11]. Fe_3O_4 was not fully reduced on the cathodic scan, even at the cathodic limit of –1.2 V in 1 M NaOH. An accumulation of irreducible products on the electrode surface built up by repetitive scans could be detected using light absorption measurements [9,10].

A similar accumulation of magnetite would account for the suppression of the current for the active region A4 in our subsequential scans, and also for the enhancement of the anodic process A3/A3' at ~ –0.5 V. With scan cycles, the charge associated with peak A3/A3' and the sum of the charges associated with peaks C1 and C2 increase together and are almost equal. This indicates that the species formed anodically in region A3/A3' are reduced in region C1 and C2. This anodic peak separates 0.05V away into two peaks (hence, the notation A3/A3') when the scan rate is reduced down to 0.1667 mV/s, confirming that two anodic processes are involved. CVs to various anodic potential limits (results not shown) indicate that peaks C1 and C2 are associated with anodic processes A3 and A3', respectively.

The sharp anodic peak A3/A3' suggests a rapid reaction to produce an insulating surface layer. Based on equilibrium potentials (Figure 3) and the stability of Fe_2O_3, the conversion of $Fe_3O_4 \rightarrow \gamma\text{-}Fe_2O_3$ is the most likely reaction. With voltammetry cycle continuing, the increase in size of peak A3 is consistent with the accumulation of Fe_3O_4 on successive cycles and its oxidation (at least partially) to γ-Fe_2O_3. The oxidation of Fe_3O_4 to γ-Fe_2O_3 should be rapid since both oxides have similar crystallographic structure. Both phases possess an O^{2-} sub lattice that is cubic close-packed (ccp), and Fe^{II}/Fe^{III} cations occupy similar octahedral and tetrahedral lattice sites [22]. Since peak A3/A3' also lies above the equilibrium potential for the conversion of $Fe(OH)_2$ to γ-FeOOH, this reaction could account for the anodic current associated with A3'. The assignment of the anodic processes (A3/A3') to the formation of Fe^{III} species (γ-Fe_2O_3 and γ-FeOOH) is consistent with the claims of Devine et.al. [23,24], who investigated the passivated films using in-situ surface-enhanced Raman spectroscopy. They suggested that the passivated film formed at low passive potential (– 0.4 V at pH = 8.4) consist of $Fe(OH)_2$, Fe_3O_4 and/or γ-Fe_2O_3 (or γ-FeOOH), whereas at higher passive potential (0.1 V at pH = 8.4) γ-FeOOH is predominant.

The two anodic peaks are attributed to the reduction of γ-FeOOH (C1) and γ-Fe_2O_3 (C2) to Fe_3O_4. Both these reduction processes can lead to the production of soluble Fe^{II} but the production of significant amounts of soluble iron is unlikely at pH = 10.6. The reduction of γ-FeOOH to Fe_3O_4 has been proved by Stratmann et.al. based on XRD and magnetic force measurements [22].

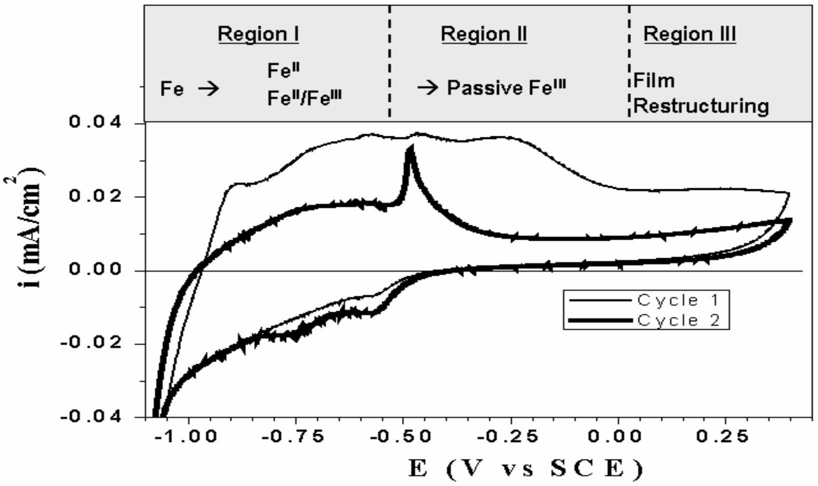

Figure 5: Summaries of the Anodic Behaviour of Carbon Steel Superimposed on a CV (from Figure 3).

Finally, a very shallow additional anodic process (A5) is observed over the potential range 0.0 to 0.4 V. it could be attributed to the conversion of Fe_3O_4 to γ-FeOOH, as suggested by the equilibrium potential in Figure 3. This assignment is consistent with the conclusions of Devine et.al. [23,24], who observed Raman peaks associated with γ-FeOOH for passivated films formed at high passive potentials. For an increase in current to be observed in this potential region, the film has to be either not completely passivated or undergoing some breakdown or re-structuring. As a large number of reactions are possible, it is not clear what causes this. One possibility is that a volume change caused by field- or stress-assisted dehydration processes (e.g., γ-FeOOH to Fe_2O_3) leads to a temporary loss of passivation. The decreasing in current of this process on successive cycles indicates either an increasing in thickness or formation of protective passivated film.

Based on the discussion above, three distinct regions as a function of potential can be specified: (I) $E < -0.5$ V; (II) $-0.5 \text{ V} < E < 0.0$ V; and (III) $E > 0.0$ V (Figure 5). In region I, anodic oxidation leads to dissolution as Fe^{2+} and formation of oxides/hydroxides in states of Fe^{II} and Fe^{II}/Fe^{III}. This is the active region for steel. The major component: $Fe(OH)_2$ and Fe_3O_4, although partially protective, are conductive and able to support cathodic reactions (e.g. the reduction of H_2O). The beginning of region II is marked by the sharp peak at ~ –0.5

V, indicating the formation of γ-Fe_2O_3 and γ-FeOOH species. Since Fe^{III} oxides/hydroxides are very insoluble, this marks the onset of passivity. However, the properties of this layer appear to vary with E and pH as can be appreciated by comparing our results with those from Schmucki et al (pH = 8.4 [9, 10]) and Hugot-Le Goff (pH = 14 [11]). In region III, film breakdown/restructuring and anodic oxidation of Fe_3O_4 to γ-FeOOH take place simultaneously.

3.2. Potentiostatic Film Growth

Films were grown at –0.15 V (in region II), 0.1 V and 0.3 V (in region III), and they were expected to be passivated. The relationship of charge (Q)-time is plotted in log values as shown in Figure 6. The changes in slope represent the current behaviour as the film gets oxidized at different potentials. The potential dependence of the current is small initially (< 1 s), which suggests a predominantly chemically controlled anodic dissolution process through a rapid growth of $Fe(OH)_2$. The thickness of $Fe(OH)_2$ varies with potential applied. As it is conductive, the current change is smaller in the region and is almost independent of potential. The subsequent fast decay in current (1 s to ~10 s) could represent the formation of a partially protective layer of Fe_3O_4 either transforming from $Fe(OH)_2$, which is a potential-dependent procedure, or the anodic oxidation from the underlying steel directly, or both of them. For t > 10s, the current is almost constant and the value is small (about 10^{-9} A), which suggests the formation of a passivated oxide/hydroxide film on carbon steel surface. The potentials we chose are more positive than the potential for peak A3/A3' in figure 4, the formation of a layer of Fe_2O_3 is possible. Fe_2O_3 is quite insoluble and a good insulator. As this passivated film get thicker, the resistance of the film increases greatly and the current decreases dramatically. At a certain level, the formation of oxide/hydroxide film reaches equilibrium with dissolution of the film. In this situation, the current is small and the value is relative constant.

From discussion above, the major components of the film after potentiostatic growth are Fe^{II}/Fe^{III} species (such as Fe_3O_4) and Fe^{III} species (such as Fe_2O_3). Fe_2O_3 is insoluble and non-conductive, while Fe_3O_4 is less soluble and semi-conductive. The differences in their physical/chemical characters will change the property of the oxide film. We will discuss about this later.

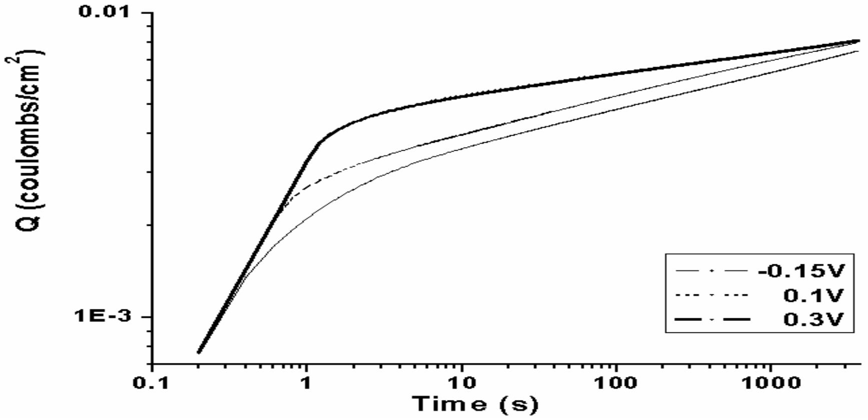

Figure 6: Net charge behaviour for potentiostatic film growth at various applied potentials.

3.3. Effect of H_2O_2 on Oxide Films

3.3.1.Corrosion Potential

Following relaxation on open circuit, concentrated H_2O_2 was added so that the concentration of H_2O_2 in the electrolyte is 10^{-3} M. The responses of E_{CORR} for films grown at –0.15 V and 0.1 V are shown in Figure 7. E_{CORR} increases sharply on addition of H_2O_2, and then changes more gradually to achieve a steady-state value, $(E_{CORR})_{SS}$. The steady-state values are the same, about ~ 0.05 V, irrespective to the potential applied to the film originally. Since $(E_{CORR})_{SS}$ is in the passivated region this suggests that addition of hydrogen peroxide leads to surface passivation regardless of the initial surface composition.

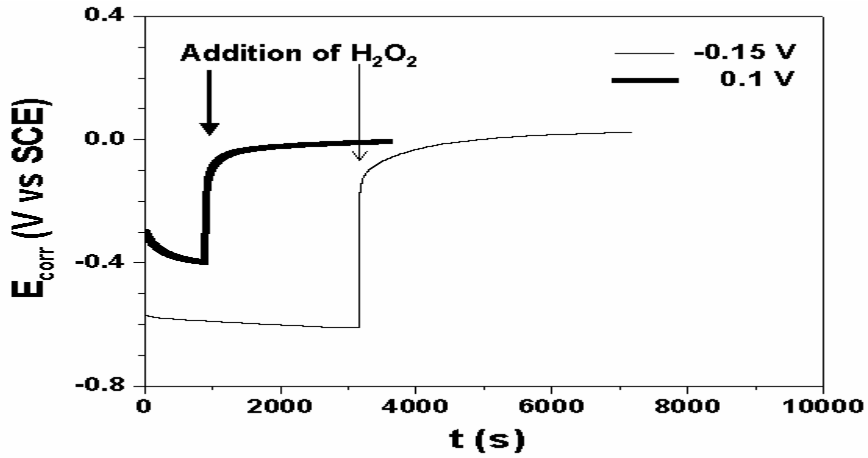

Figure 7: Time Dependent Behaviour of E_{CORR} on Oxide-Covered Carbon Steel Following the Addition of 10^{-3} M H_2O_2: Films Grown for 1 h at –0.15 and at 0.1 V

3.3.2.Electrochemical Impedance Spectroscopy

EIS spectra, as shown in Figure 8, were obtained on films grown at –0.15 V (in region II) and 0.1 V (in region III) before and after exposure to 10^{-3} M H_2O_2. The time-dependent behaviour of the spectra reflects that: a rapid initial change on films in addition of H_2O_2, followed by a slow change over time. As we discussed before, the composition of the

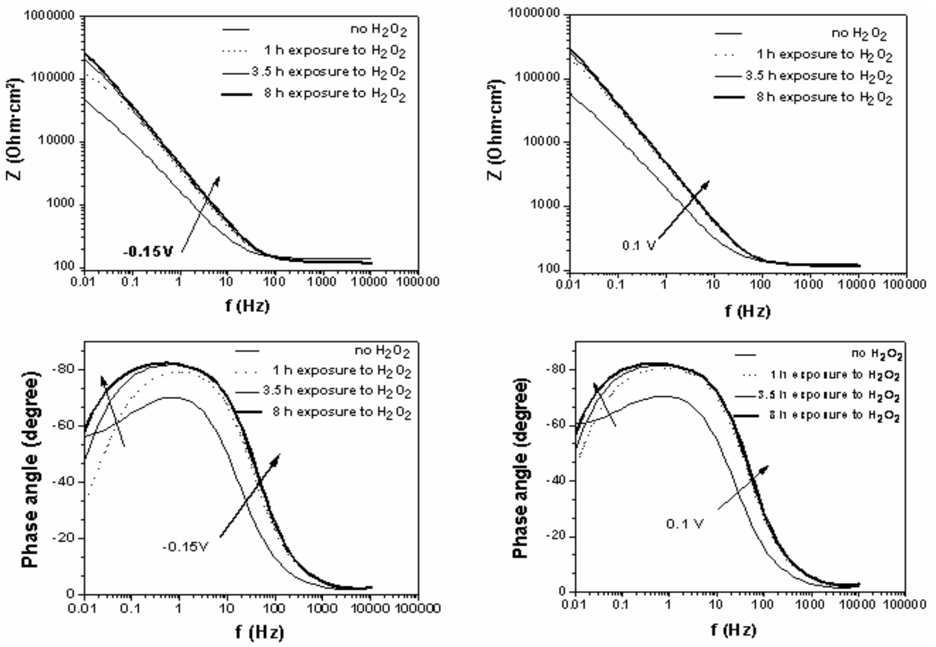

Figure 8: Electrochemical Impedance Spectra of Carbon Steel Electrodes Covered with Potentiostatically Grown Oxide Films. The films were grown at – 0.15 V and 0.10 V,

allowed to relax for 20 min and then exposed to a solution containing 10^{-3} M H_2O_2. The EIS spectra were taken at exposure times of 1.4 h, 4 h and 8.5 h.

Passivated film is made of Fe^{II}/Fe^{III} species. A layer of reactive $Fe(OH)_2/Fe_3O_4$ covered by a layer of Fe_2O_3/FeOOH and the properties of these two layers are different. An electrical equivalent circuit involving two parallel RC circuits in series was found in most spectra fitting [25]. Such a circuit is consistent with the scheme of a dual layer film grown potentiostatically as illustrated in Figure 9. In this circuit, τ_2 (= $R_2(CPE)_2$) represents the charge transfer processes within the inner $Fe(OH)_2/Fe_3O_4$ layer, and τ_1 (= $R_1(CPE)_1$) represents the migration processes in the outer passivated Fe_2O_3/FeOOH layer. Analysis according to this circuit yields the parameter values given in Table 1. The parameter, p_{CPE}, is the exponent defining the nature of the constant phase element (CPE) used to fit the circuit. A value of p_{CPE} approaching 1 defines CPE as effectively a capacitance. For CPE1, p_{CPE1} is often larger than 1 and in those cases a value = 1 was fixed when performing the fit, thus, CPE1 was assumed to be a capacitance in subsequent discussions. For CPE2, p_{CPE2} is always > 0.8 and CPE2 was taken to be a capacitance.

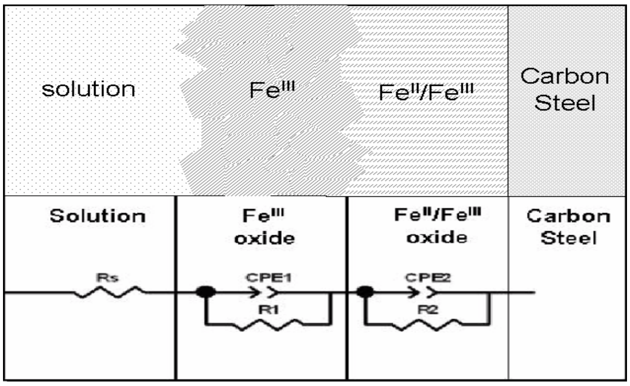

Figure 9: Schematic Representation of the Anodically Grown Dual Layer Film and the Electrical Equivalent Circuit Used in EIS Analyses: Films Grown at –0.15 V and 0.1 V.

Table 1: Fitting parameters of the equivalent circuit analysis of the EIS results

Film Growth Potential	Exposure time to H_2O_2	Rs (Ω•cm^2)	R2 (Ω•cm^2)	CPE2 (F/cm^2)	p_{CPE2}	R1 (Ω•cm^2)	CPE1 (F/cm^2)	p_{CPE1}
–0.15 V	0	133	1.0E4	2.0E-5	0.82	1.5E5	2.6E-4	0.88
	1	118	5.4E4	8.0E-5	0.88	0.9E5	1.4E-4	1
	3.5	118	4.7E4	1.1E-4	0.85	2.6E5	7.2E-5	1
	8	118	4.5E4	1.2E-4	0.84	5.0E5	5.9E-5	1
0.1 V	0	122	1.2E4	2.3E-4	0.81	3.0E5	2.0E-4	0.88
	1	116	4.9E4	9.5E-5	0.85	2.5E5	7.3E-5	1
	3.5	115	4.6E4	1.1E-4	0.84	3.8E5	5.8E-5	1
	8	114	4.2E4	1.2E-4	0.83	5.4E5	5.1E-5	1

Figure 10(a) suggests that: the resistance of the inner oxide layer (R_2) increases sharply on addition of H_2O_2, and then decreases very slightly with time. This accompanies with a sharp decrease initially in C_2 followed by a subsequent slow increase. It could be explained as a sudden thickening in the inner Fe^{II}/Fe^{III} oxide/hydroxide layer, which must involve further oxidation of the steel surface driven by H_2O_2 reduction. In figure 10(b), the resistance of the outer layer (R_1) initially decreases slightly, then increases steadily over the subsequent 8 h exposure period. This increase in R_1 is accompanied by a steady decrease in capacitance (C_1). The decrease in R_1 at the beginning indicates that the addition of H_2O_2 leads to a more defective outer layer thereby allows the inner layer to grow. As time passing, the steady increase in R_1 (and decrease in C_1) indicates a slow re-passivation process. The slight decrease in R_2 and slow increase in R_1 is consistent with the growth of the outer layer via conversion of the inner layer, i.e. oxidizing of $Fe_3O_4/Fe(OH)_2$ to $Fe_2O_3/FeOOH$. The increase in the outer layer resistance (and corresponding decrease in capacitance) reflects a combination of film thickening (at the expense of the inner layer) and film passivation.

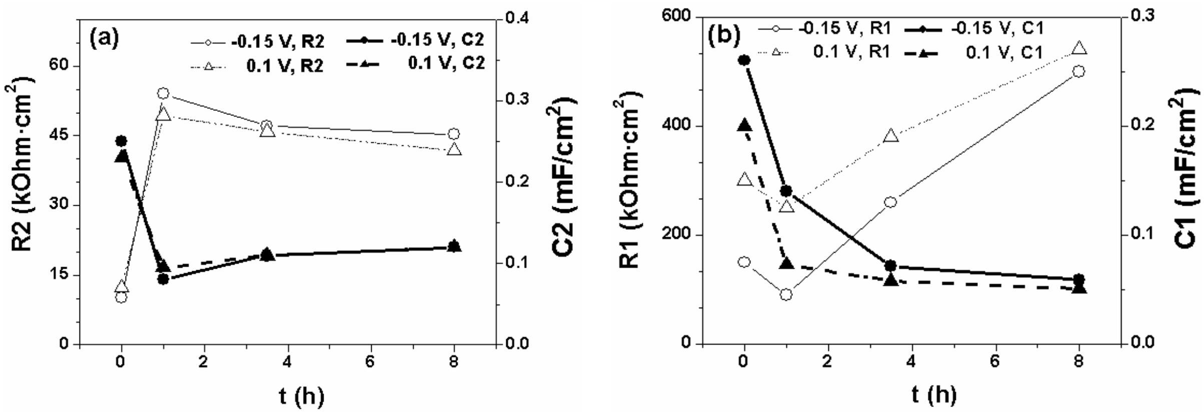

Figure 10: Film Resistances and Capacitances Obtained by Fitting to the Electric Equivalent Circuit Analysis in Figure 9: (a) the inner layer; and (b) the outer layer.

3.4 Surface Analyses

The oxidized surface sample was analysed by ex-situ analyses. Although, being exposed to air prior to analysis, the sample is careful handled under low oxygen environments trying to minimize any changes and introduction of contaminations. Also, the films, formed at the high potentials (> –0.2 V), are relatively inert with the surface already oxidized predominantly to the Fe^{III} state. The Raman spectrum of a sample preoxidized at + 0.4V is shown in Figure 12. The peaks are very weak on such a smooth surface. Other oxides/hydroxides were likely present, but the quantity to be detected by Raman spectroscopy is not sufficient. The variation observed between different areas of the same sample is relatively large. There appears to be a measurable increase in the Raman scattering peak for Fe_3O_4 as a result of exposure to H_2O_2 of a specimen preoxidized at +0.4V. This is consistent with the claim (above) that exposure to H_2O_2 leads initially to a degradation of the passivated layer leading to growth of the inner layer.

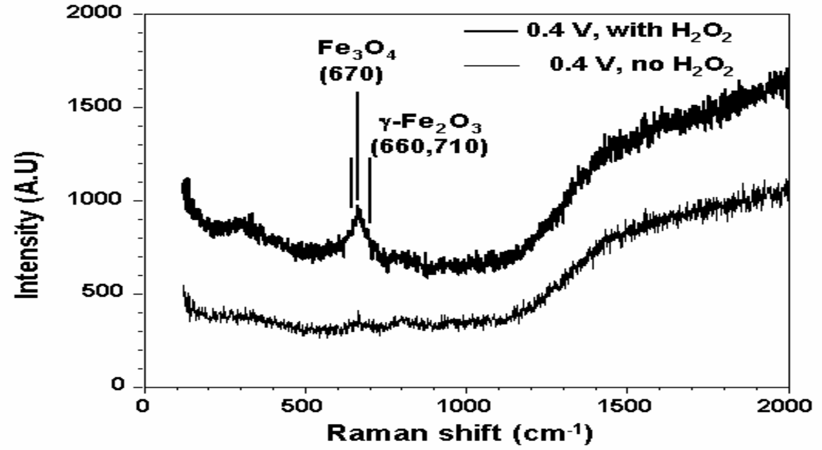

Figure 12: Ex-situ Raman Spectra Obtained with Films Grown at 0.4 V: the lower spectrum is for a film before exposed to H_2O_2 while the upper spectrum is for the film after

exposed to 10^{-3} M H_2O_2. The lines indicate the main Raman shifts (in cm^{-1}) expected for Fe_3O_4 and γ-Fe_2O_3

4. Conclusions

Based on cyclic voltammetry experiments, the anodic behaviour of carbon steel in borate solutions (pH = 10.6) can be divided into three distinct regions: (I) potential region < -0.5 V, when the surface is active and partially covered by $Fe(OH)_2/Fe_3O_4$; (II) potential region –0.5 V to ~ 0 V, when the surface is passivated with an outer layer of Fe_2O_3/γ-FeOOH over the inner Fe^{II}/Fe^{III} oxide/hydroxide layer; (III)potential region > 0 V, within which the further conversion of Fe_3O_4 to γ-FeOOH can cause some restructuring and slight film breakdown.

Potentiostatics and EIS results are consistent with a film comprised of a dual layer structure with an outer layer of Fe^{III} oxide/hydroxide covers an inner layer of Fe^{II}/Fe^{III} oxide/hydroxide. Raman spectroscopy indicates the inner layer is predominantly Fe_3O_4.

Addition of 10^{-3} M H_2O_2 leads the outer passivation layer to degrade initially and the inner layer to thicken; then, followed by the slow repairing of the outer layer as its Fe^{III} content steadily increases with time. A stronger signal for Fe_3O_4 in the Raman spectrum is consistent with an inner layer thickening.

5. Acknowledgement

This research was funded under the Natural Science and Engineering Council of Canada (NSERC) and Atomic Energy of Canada Limited (AECL) Industrial Research Chair Agreement. The electrochemical analysis equipment was purchased by a grant from the Canada Foundation for Innovation. Surface Science Western is greatly acknowledged for their assistance in performing surface analyses. I would like to thank Professor Shoesmith and Dr. X. Zhang for their support and discussion throughout the project.

6. References

1. Spinks, J. W. T.; Woods, R. J. *An Introduction to Radiation Chemistry.* 3rd Ed. (1990), pp. 592.
2. Ishigure, Kenkichi; Nukii, Takashi; Ono, Shoichi. Analysis of water radiolysis in relation to stress corrosion cracking of stainless steel at high temperatures - Effect of water radiolysis on limiting current densities of anodic and cathodic reactions under irradiation. *Journal of Nuclear Materials* Vol. 350, Iss. 1, (2006), pp. 56-65.
3. Lin, C. C.; Kim, Y. J.; Niedrach, L. W.; Ramp, K. S. Electrochemical corrosion potential models for boiling-water reactor applications. *Corrosion (Houston)* Vol. 52, Iss. 8, (1996), pp. 618-625.
4. R.M. Cornell and U. Schwertmann, The iron oxides, 2nd edition, Wiley-Vch Gmbh, 210 (2000).
5. D.J. Jobe, R. J. Lemire and P. Taylor, Iron oxide redox chemistry and nuclear fuel disposal, AECL-11667, COG-96-487-1 (1997).
6. D.J. Jobe, The calculated solubilities of hematite, magnetite and lepidocrocite in steam generator feedtrains, AECL-11683 (1997).
7. T. Misawa. The Thermodynamic Consideration For Fe-H_2O System at 25°C. *Corros. Sci*, Vol. 13, (1973), pp. 659.

8. Silverman, David C.. Presence of solid ferrous hydroxide in EMF-pH diagram for iron. *Corrosion (Houston, TX, United States)* Vol. 38, Iss. 8, (1982), pp. 453-5.

9. Buchler, M.; Schmuki, P.; Bohni, H. Iron passivity in borate buffer. Formation of a deposit layer and its influence on the semiconducting properties. *Journal of the Electrochemical Society* Vol. 145, Iss. 2, (1998), pp. 609-614.
10. Buchler, M.; Schmuki, P.; Bohni, H. Formation and dissolution of the passive film on iron studied by a light reflectance technique. *Journal of the Electrochemical Society* Vol. 144, Iss. 7, (1997), pp. 2307-2312.
11. Hugot-Le Goff, A.; Flis, J.; Boucherit, N.; Joiret, S.; Wilinski, J. Use of Raman spectroscopy and rotating split ring disk electrode for identification of surface layers on iron in 1M sodium hydroxide. *Journal of the Electrochemical Society* Vol. 137, Iss. 9, (1990), pp. 2684-90.
12. W.J. Lorenz and K.E. Hensler, in Corrosion Mechanisms (ed't F. Mansfeld) Marcel Dekker Inc., New York, Chapter 1 (2003).
13. Castro, E. B.; Vilche, J. R.; Arvia, A. J. Iron dissolution and passivation in potassium carbonate-potassium bicarbonate solutions. Rotating ring disk electrode and XPS studies. *Corrosion Science*, Vol. 32, Iss. 1, (1991), pp. 37-50.
14. Castro, E. B.; Valentini, C. R.; Moina, C. A.; Vilche, J. R.; Arvia, A. J. The influence of ionic composition on the electrodissolution and passivation of iron electrodes in potassium carbonate-bicarbonate solutions in the 8.4-10.5 pH range at 25°C. *Corrosion Science* Vol. 26, Iss. 10, (1986), pp. 781-93.
15. Flis, J.; Zakroczymski, T.. Enhanced hydrogen entry in iron at low anodic and low cathodic polarizations in neutral and alkaline solutions. *Corrosion (Houston, TX, United States)* Vol. 48, Iss. 7, (1992), pp. 530-9.
16. Bockris, J. O'M.; Drazic, D.; Despic, A. R. Electrode kinetics of the deposition and dissolution of iron. *Electrochimica Acta* , Vol. 4, (1961), pp. 325-61.
17. Bockris, J. O'M.; Kita, Hideaki. Analysis of galvanostatic transients and application to the iron electrode reaction. *Journal of the Electrochemical Society* Vol. 108, (1961), pp. 676-85.
18. Bockris, J. O'M.; Drazic, D. Kinetics of deposition and dissolution of iron: effect of alloying impurities. *Electrochimica Acta* Vol. 7, (1962), pp. 293-313.
19. Geana, D.; El Miligy, A. A.; Lorenz, W. J.. Electrochemical behavior of iron in alkaline sulfate solutions. *Journal of Applied Electrochemistry* Vol. 4, Iss. 4, (1974), pp. 337-45.
20. Schrebler, Guzman R. S.; Vilche, J. R.; Arvia, A. J.. The potentiodynamic behavior of iron in alkaline solutions. *Electrochimica Acta* Vol. 24, Iss. 4, (1979), pp. 395-403.
21. Ohtsuka, T.; Ju, J.-C.; Ito, S.; Einaga, H.. The composition of Fe(III) oxy-hydroxide film anodically deposited in borate solution. *Corrosion Science* Vol. 36, Iss. 7, (1994), pp. 1257-66.
22. Stratmann, M.; Bohnenkamp, K.; Engell, H. J. An electrochemical study of phase transitions in rust layers. *Corrosion Science* Vol. 23, Iss. 9, (1983), pp. 969-85.
23. Gui, J.; Devine, T. M. A SERS investigation of the passive films formed on iron in mildly alkaline solutions of carbonate/bicarbonate and nitrate. *Corrosion Science* Vol. 37, Iss. 8, (1995), pp. 1177-89.
24. Schroeder, Valeska; Devine, Thomas M.. Surface enhanced Raman spectroscopy study of the galvanostatic reduction of the passive film on iron. *Journal of the Electrochemical Society* Vol. 146, Iss. 11, (1999), pp. 4061-4070.

25. Alves, Valeria A.; Brett, Christopher M. A. Characterization of passive films formed on mild steels in bicarbonate solution by EIS. *Electrochimica Acta* Vol. 47, Iss. 13, (2002), pp. 2081-2091.